

Vibrational Coherence from the Dipyridine Complex of Bacteriochlorophyll *a*: Intramolecular Modes in the 10–220-cm⁻¹ Regime, Intermolecular Solvent Modes, and Relevance to Photosynthesis

Katherine R. Shelly, Elizabeth A. Carson, and Warren F. Beck*

Department of Chemistry, Michigan State University, East Lansing, Michigan 48824

Revised August 1, 2003; E-mail: beck@cem.msu.edu

Supporting Material

Experimental

Dynamic-absorption spectroscopy was performed with a femtosecond pump-probe spectrometer consisting of a self-mode-locked titanium–sapphire oscillator and a rapid-scanning Mach-Zehnder interferometer. An early version of the spectrometer was discussed previously,^{1,2} and the current version was described in a more recent paper.³ Some significant recent changes that led to improved sensitivity and reproducibility are described here.

A Mira 9000 oscillator (Coherent) that was equipped with X-wave broad-tuning-range cavity optics was used in these experiments. The oscillator was pumped by a Verdi (Coherent) 5-W laser. The output pulses were used at the natural pulse-repetition rate (75 MHz), without pulse selection. Extracavity pulse compression and group-velocity-dispersion precompensation was accomplished with a double-passed pair of SF10 prisms. The prism separation was adjusted to minimize the pump–probe autocorrelation width at the position of the reference nonlinear crystal (*vide infra*), which was confocal with the sample position.

The detection system employed a rapid-scanning,⁴ modified Mach-Zehnder interferometer¹ of an improved design. A galvanometer-driven translation stage and retroreflector (Clark-MXR ODL-150) was used to scan the pump-pulse time-of-flight delay at a 1.3-Hz repetition rate over a 12-ps range. The pump beam was amplitude modulated at 100 kHz by a $\lambda/2$ -retarding photoelastic modulator (Hinds Instruments) and a Glan-laser calcite polarizer (Karl Lambrecht). The probe beam's

plane of polarization was analyzed at 45° with respect to the pump beam's plane of polarization by a Glan-laser calcite polarizer; a mica zero-order $\lambda/2$ plate (Karl Lambrecht) prior to the polarizer was rotated to control the probe intensity. A BK7 lens with a focal length of 10 cm was used to focus the pump (125 pJ/pulse) and probe beam (30 pJ/pulse) onto the sample's position.

After transmitting the sample and after recollimation, the probe beam was analyzed at 90° with respect to the pump polarization by another Glan-laser calcite polarizer. The transmitted probe beam was then passed through a monochromator (Acton Research SpectraPro 150, 2-nm spectral band pass) and detected by a amplified silicon photodiode (Thorlabs PDA520). The photodiode signal was demodulated by a digital lock-in amplifier (SRS 750, Stanford Research Systems), which was referenced to the 100-kHz pump-modulation frequency.

The lock-in amplifier was operated in a differential detection mode, with the transmitted-probe photodiode signal balanced by that from a reference photodiode. The reference photodiode was used to detect a variable sum of a very small portion of the pump and probe beams, which were split from the main beams prior to the sample-focusing lens by an antireflection-coated compensator plate. The intensity of the pump-beam fraction on the reference photodiode was adjusted with a variable-density neutral-density filter to cancel the post-time-zero bleaching signal at some point in the probe-delay scan; the unmodulated probe beam was used to bias the reference photodiode into the operating regime used by the sample-beam's photodiode. This practice improved the signal/noise ratio significantly by allowing a partial nulling of the noise arising from the oscillator and pump laser.

The pump and probe beams were sampled prior to the focusing lens to provide a pair of reference pulses for autocorrelation analysis during data acquisition. A β -barium borate crystal (Inrad or Cleveland Crystals, 100- μm thickness, cut for type I sum-frequency generation with 800-nm input) was placed at the focus of a 10-cm focal-length BK7 lens; the second-harmonic beam was detected by a photomultiplier tube and lock-in amplifier (LIA-MV-200-H, Femto Messtechnik). The group-delay dispersion in the autocorrelation arm of the interferometer was the same as in the sample arm; identical beam splitters, compensator plates, and focusing optics were employed. A

sample/hold amplifier and digitizer (National Instruments SC-2040 S/H and PCI-6024E, respectively) simultaneously acquired at a 17-kHz sampling rate the analog output of the pump-probe and autocorrelation lock-in amplifiers and the galvanometer's position signal, resulting in 7000 points per scan; the effective dwell time per acquired data point was 1.8 fs. The signal-averaging system and monochromator were controlled by LabView routines. We eliminated scan-to-scan delay drift by employing the autocorrelation signal as a zero-delay-time reference pulse for each scan; in previously reported rapid-scanning experiments, a modest broadening of the instrument-response function was observed in long averaging runs.^{1,5}

Results

Pump-Probe Signals from Bacteriochlorophyll *a* and Pyridine

In this section, we consider in detail how much the pyridine solvent contributes to the BChl pump-probe signal. Figure 4 compares the pump-probe signal obtained at room temperature from bacteriochlorophyll *a* (BChl) in pyridine solvent with the signal obtained under the same experimental conditions from neat pyridine solvent. Note that the y axes of the two graphs are set up so that the relative intensities of the two signals can be determined by inspection. The discussion that follows shows that we can neglect any contribution of the *nonresonant* oscillatory signal from pyridine to the signals shown in figure 1–3.

The Bchl pump-probe signal shown in figure 4 is the same one used in figures 1–3. The most intense feature is the bipolar pump-probe coherence spike near the zero of time. This spike is superimposed on the pump-induced change in transmittance that can be attributed to the change in ground-state population arising from the $\pi \rightarrow \pi^*$ transition; the intensity change from the baseline prior to time zero and nondecaying ($\tau > 1$ ns) fraction corresponds to a $\Delta T/T$ of 10^{-4} . As stated in the caption to figure 1, the the full range of the oscillatory signal used in figure 1 and in the subsequent analysis of the components of the vibrational coherence is perhaps ten percent as large, a $\Delta T/T$ of 10^{-5} . In terms of the relative-intensity units used in figures 1 and 4, there is a full-scale

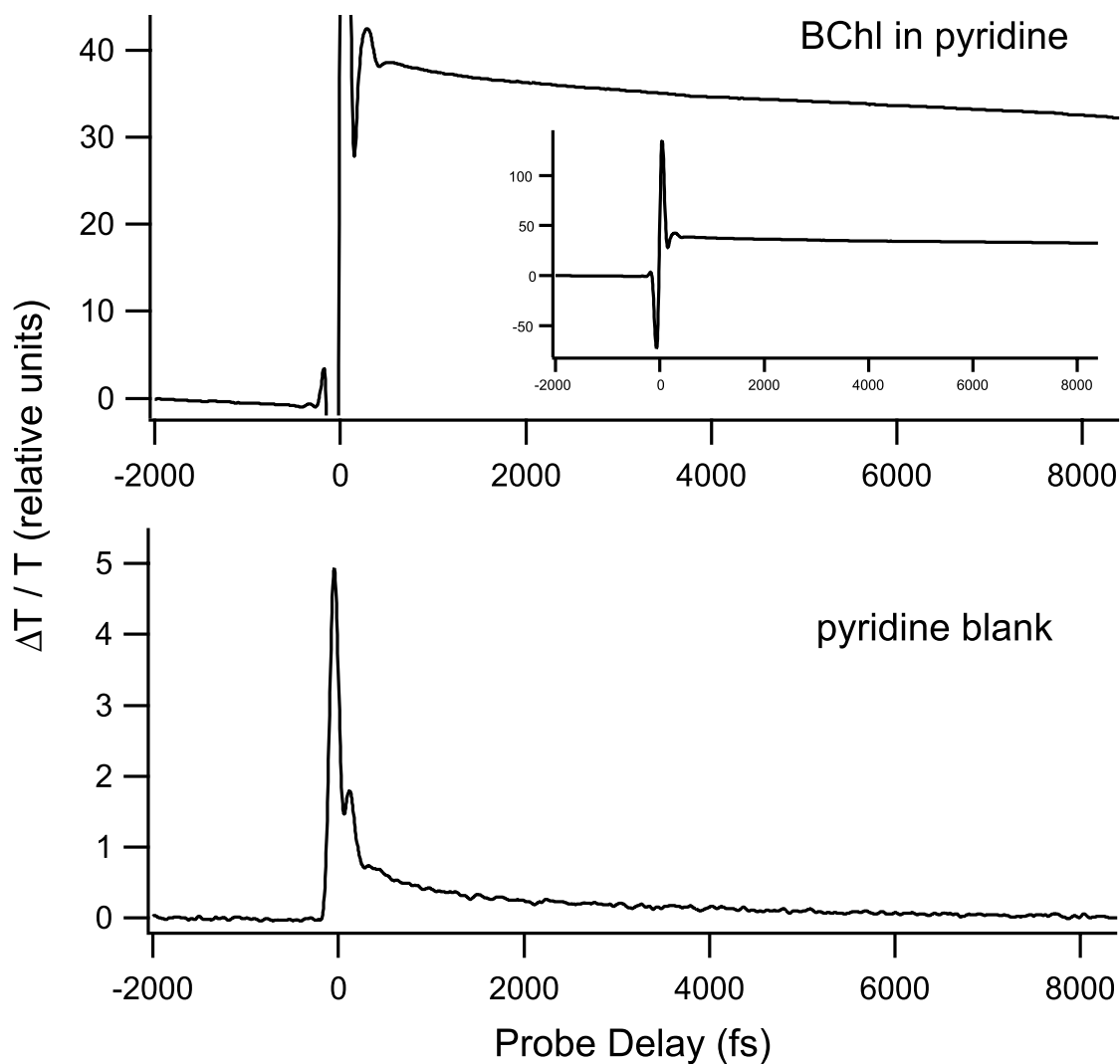


Figure 4. Pump–probe signal obtained under the same instrumental conditions from BChl in pyridine solvent (average of 27,000 scans) and in neat pyridine (average of 70,000 scans). The inset shows the full amplitude range of the BChl signal, keeping the zero-time coherence spike on scale, whereas the main graph shows the range corresponding to the population change in the BChl ground state. The y axes employ a consistent relative-intensity scaling. The BChl signal was treated using the methods of the following section to obtain figures 1–3.

modulation of about 2.5 units.

The pump–probe signal observed in neat pyridine arises from the optical-Kerr effect (OKE). It exhibits a spike near the zero of time that arises from the nonresonant electric hyperpolarizability, a weak beating modulation near the 150-fs time point, and a subsequent exponential decay that arises from diffusive reorientational relaxation. The signal is very similar in shape to that reported in the past by McMorrow and Lotshaw,⁶ but the laser pulses used in our experiment are shorter in duration. The signal/noise ratio of our signal is poor compared to that of the McMorrow and Lotshaw signal, even after many hours of signal averaging, because we detect the signal against a large transmitted-probe background. (The best technique for detection of nonresonant OKE signals is to rotate the probe-analyzing polarizer so that it is crossed (obtaining maximum extinction) against the probe’s plane of polarization; then, by a small rotation of a $\lambda/4$ retarder plate or of the analysis polarizer, a small leakage signal from the probe is admitted to obtain optical-heterodyne detection (OHD) conditions. So, the OHD-OKE signal is detected essentially against a zero background, and the signal/noise ratio is appropriately much better than that obtained under our conditions. In effect, our analysis polarizer is rotated way beyond the limit needed to obtain full heterodyning.) Our intention, here, of course, is not to record the OHD-OKE signal but to obtain a valid estimate of how much the pyridine solvent itself contributes a *nonresonant* background signal in the pump–probe experiment with BChl present, under the same optical conditions.

Over the time range from 150 fs to 7 ps shown in figure 1, the pyridine blank exhibits at full-range modulation of much less than 1 relative-intensity unit. Figure 4 shows that the significant OKE modulations observed in pyridine occur at shorter delay times and exhibit a different intensity profile than those observed in the BChl/pyridine sample. Further, the BChl and pyridine-OKE modulation spectra are not the same. The pyridine OKE spectrum (not shown), obtained using the methods of the next section, exhibits a peak in the 60–90-cm⁻¹ regime and substantial intensity in the 0–60-cm⁻¹ region; considering the effects of our shorter laser pulses, the spectrum is consistent with that reported previously by McMorrow and Lotshaw.⁶

A direct comparison of intensities between the BChl and pyridine-blank sample is not appro-

appropriate because it does not account for the attenuation of the laser intensity in the BChl sample. In the BChl pump–probe experiment, the absorbance was 0.6 at the center of the laser spectrum. With respect to the background pyridine OKE signal, the presence of BChl contributes an attenuation of the laser fluence for the pump and probe beams *and* it attenuates the exiting third-order polarization signal (the OKE signal) beam to the same degree. Accordingly, in the presence of BChl, the background pyridine OKE signal is approximately $(10^{-0.6})^3 = 1.6 \times 10^{-2} = \frac{1}{63}$ as large as that observed in neat pyridine. Given the very small amplitude of this signal over the range of the BChl signal that is shown in figure 1, it is certainly safe to ignore the presence of the OKE signal in the analysis.

Data Analysis

Fourier-Magnitude Spectrum Estimation

The oscillatory fraction of the pump–probe signal (see figure 1) was obtained by subtracting a fitted triple-exponential function from the signal segment starting well beyond the pump–probe coherence spike, at the 150-fs delay point, and extending to the end of the acquired signal. It was then multiplied by a Hanning (or raised cosine) window function,⁷

$$w(k) = 0.5 \left(1 - \cos \left(\frac{2\pi k}{n+1} \right) \right) \quad (1)$$

defined for the point index k in the data segment in terms of the number of data points n . The window function gradually forces the intensity at the beginning and end of the signal segment to zero amplitude. This procedure is required to suppress satellite ripples in the Fourier-magnitude spectra, which arise from leakage of signal frequencies into adjacent channels owing to truncation of the time-domain signal at the beginning and end. The window function also causes a broadening of the observed signal line shape at a given frequency, but this same broadening can be applied in simulation of the frequency-domain spectrum to return accurate damping constants. Next, the

windowed signals were zero-padded by a factor of 32 in order to enhance the point density along the frequency axis in the Fourier-magnitude spectra. Lastly, the spectrum was compensated for the finite width of the instrument-response function by deconvolution in the frequency domain: the raw magnitude was scaled by the reciprocal of the Fourier magnitude at frequency ω_i obtained from the pump-probe autocorrelation signal.⁸

The reader should take note that the deconvolution step mentioned above causes the signal/noise to deteriorate as the frequency increases. This effect arises from the need to have the laser pulses be much shorter than the period of a given mode's vibrational period. With our 50-fs pulses, we find that we cannot reproduce features in the Fourier-magnitude spectrum above 220 cm^{-1} . At that point, the power in the pump-probe autocorrelation function is about 50 percent of that at 0 cm^{-1} .

The resolution of the Fourier-magnitude spectrum is determined by the length of the analyzed time-domain data segment and the windowing function. Using the modulated portion of the BChl signal shown in figure 1, the effective resolution in the calculated Fourier-Magnitude spectrum is 10 cm^{-1} .

Modeling of the Underdamped Components

The parameters listed in table 1 were obtained by a robust frequency-domain modeling procedure.³ The experimental Fourier-magnitude spectrum (figure 2) was modeled using a sum of damped cosines,

$$I(t) = \sum_i A_i e^{-t/\gamma_i} \cos(\omega_i t + \phi_i). \quad (2)$$

The model signal was sampled using the delay times t and segment lengths obtained from the experimental signal (see figure 1); it was processed by the same sequence of windowing, zero-padding, and Fourier-magnitude spectrum calculation. The intensities A_i , frequencies ω_i , and damping times γ_i were adjusted iteratively to reproduce the intensity, position, and width of each significant feature in the experimental Fourier-magnitude spectrum. Note that the phases ϕ_i are optionally obtained by optimization of the model in the time domain. The components that were

included in the model are those that were reproduced in frequency and relative intensity in a set of replicate experiments.

Table 1: Frequencies, normalized deconvolved intensities,^a and damping constants for the under-damped oscillatory components^b observed in the pump–probe signal from bacteriochlorophyll *a* in pyridine solvent

Frequency (cm ⁻¹)	11	33	49	59	68	80	103	116	138	169	182	206
Intensity ^a	1.00	0.09	0.03	0.02	0.03	0.03	0.02	0.04	0.26	0.12	0.18	0.16
γ (fs)	800	1100	1500	1700	1500	1500	1700	1500	1000	1200	1200	1300

^arelative to the magnitude of the 11-cm⁻¹ component after deconvolution in the frequency domain

^bmodeled by a sum of damped cosinusoids, $\sum_i A_i \exp(-t/\gamma_i) \cos(\omega_i t)$

Modeling of the Rapidly Damped Component

The rapidly damped modulation component observed over the 200–600-fs time region (see figures 1 and 3) was modeled using a distribution of cosinusoidal components defined by the sum of two lognormal (asymmetric Gaussian)⁹ distribution functions, resulting in a model signal that closely approximates the time-domain signal (see figure 3). The distribution was sampled at 5-cm⁻¹ intervals from 1 cm⁻¹ to 1000 cm⁻¹. The intensity of the distribution at each sampling point was used as the scaling factor for a damped cosinusoid, as in equation 2, above. The damping factor for each component was arbitrarily fixed at 1 ps; changing this parameter (say, to 2 ps) had little effect on the time-domain signal obtained by summing over the entire distribution.

The parameters for the two lognormal components were iteratively adjusted until a close facsimile of the observed signal was obtained (see the top panel of figure 3). The final parameters are listed in the following table. Note that no physical significance is attributed to these parameters at this time other than that the overall distribution obtained from the sum of the two components provides an adequate description of the observed signal.

Table 2: Log-normal line shape parameters for the solvent-mode distribution

Component	Amplitude	Frequency (cm ⁻¹)	Width (cm ⁻¹)	Skew
1	0.68	145	35	1.2
2	1	175	47	1.2

References

- (1) Diffey, W. M.; Beck, W. F. *Rev. Sci. Instrum.* **1997**, *68*, 3296–3300.
- (2) Diffey, W. M.; Homoelle, B. J.; Edington, M. D.; Beck, W. F. *J. Phys. Chem. B* **1998**, *102*, 2776–2786.
- (3) Carson, E. A.; Diffey, W. M.; Shelly, K. R.; Lampa-Pastirk, S.; Dillman, K. L.; Schleicher, J. M.; Beck, W. F. *J. Phys. Chem. A* **2003**, submitted.
- (4) Edelstein, D. C.; Romney, R. B.; Scheuermann, M. *Rev. Sci. Instrum.* **1991**, *62*, 579–583.
- (5) Feldstein, M. J.; Vöhringer, P.; Scherer, N. F. *J. Opt. Soc. Am. B* **1995**, *12*, 1500–1510.
- (6) McMorrow, D.; Lotshaw, W. T. *Chem. Phys. Lett.* **1993**, *201*, 369–376.
- (7) Press, W. H.; Flannery, B. P.; Teukolsky, S. A.; Vetterline, W. T. *Numerical Recipes: the Art of Scientific Computing*; Cambridge University Press: Cambridge, 1986.
- (8) McMorrow, D.; Lotshaw, W. T. *Chem. Phys. Lett.* **1990**, *174*, 85–94.
- (9) Siano, D. B.; Metzler, D. E. *J. Chem. Phys.* **1969**, *51*, 1856–1861.